MENTORSHIP, SCHOLARSHIP, AND SERVICE: A SPECIAL ISSUE HONOURING PROFESSOR ADAMU N. BABA-KUTIGI, FNIP ON HIS RETIREMENT
FUDMA Journal of Sciences (FJS)
ISSN online: 2616-1370
ISSN print: 2645 - 2944
Vol. 10 ANB Special Issue, 2026, pp 196 – 203
DOI: https://doi.org/10.33003/fjs-2026-10(ANB-K)-5402

Numerical Optimization of ZnO Electron Transport Layer and Absorber Properties with Temperature Effects in Germanium-Based Perovskite Solar Cells Using SCAPS-1D Simulation

***[1]Dahiru M. Sanni, [2]Hadiza H. Ndanusa and [3]Hamza Abubakar A.**

[1]Department of Physics, Federal University Dutsin-Ma, PMB 5001, Dutsin-Ma, Katsina State, Nigeria.
[2]Department of Physics, Ibrahim Badamasi Babangida University, Lapai, Niger State, Nigeria.
[3]Department of Geophysics, Federal University Dutsin-Ma, PMB 5001, Dutsin-Ma, Katsina State, Nigeria.

*Corresponding authors' email: dahirusanni@gmail.com

ABSTRACT
Perovskite solar cells (PSCs) have made significant advances in power conversion efficiency (PCE); however, their commercial viability remains hindered by stability concerns with organic transport layers and the environmental toxicity of lead-based absorbers. This study investigates a lead-free germanium-based perovskite solar cell ($CH_3NH_3GeI_3$) with inorganic charge transport layers of zinc oxide ZnO and copper iodide CuI as electrons and holes transport layers, respectively, using SCAPS-1D simulation. The device design consists of FTO/ZnO/ $CH_3NH_3GeI_3$/CuI/Au in a standard n-i-p configuration. Key parameters were extensively optimized, including absorber layer thickness (300-800 nm), absorber layer bandgap (1.2-1.6 eV), ZnO electron transport layer (ETL) thickness (10-400 nm), and ZnO bandgap (2.0-4.0 eV). The results show that an optimal absorber thickness of 500-600 nm and an optimal bandgap of 1.4-1.5 eV produce a maximum PCE of about 24.9% at a temperature of 300 K. While differences in ZnO thickness have little effect on open-circuit voltage (Voc) and fill factor (FF), parasitic absorption causes small reductions in short-circuit current density (Jsc) and PCE. Increasing the ZnO bandgap improves device transparency while modestly improving performance. Temperature analysis (290-360 K) shows a considerable decrease in Voc, FF and PCE as temperature increase, whereas Jsc remains almost constant, indicating recombination dominated thermal degradation in Ge-based PSCs. Overall, this study demonstrates that optimizing inorganic transport layers and absorber layer can significantly increase the efficiency and stability of lead-free PSCs, providing valuable insights for creating environmentally friendly and thermally robust solar systems.

Keywords: Perovskite solar cells, Germanium-based perovskite, SCAPS-1D, Electron transport layer (ZnO), Thermal stability, Lead-free, Inorganic transport layers

INTRODUCTION

The perovskite solar cells (PSCs) have attracted great research interest since they were first introduced as a light absorber in 2009 by Miyasaka and his co-workers, with a power conversion efficiency (PCE) of 3.8% to their current value of about 26% (National Renewable Energy Laboratory (NREL), 2025). The high research interest is mainly due to the numerous advantages, which include low cost of production, high-power conversion efficiency (PCE), tuneable bandgap, large diffusion length, high optical absorption, and low excitation binding energy (Kim et al., 2012; Lee et al., 2012; Xing et al., 2013).

The PSCs have different architectures, and so many investigations have been carried out on the different types of architecture. Some of the architectures are mesoporous perovskite solar cells and planar heterojunction PSCs. The planar heterojunction has the simplest structure and a lower processing temperature because of the absence of mesoporous materials. There are two types of planar heterojunction PSCs, viz., the regular N-I-P and the inverted P-I-N architecture (Koech et al., 2021; Sanni et al., 2021). In the regular architecture, light enters the solar cells from the electron transport layer, and in the inverted architecture, light enters the solar cells from the hole transport layer, as shown in Fig. 1. The inverted planar architecture has been reported to eliminate hysteresis, which is usually common with the mesoporous structure during I-V measurement (Sanni et al., 2019).

Both the mesoporous architecture and the planar architectures have demonstrated high PCE. However, one major issue hindering the commercialisation of the PSCs is the issue of stability when exposed to UV, moisture, and other environmental conditions; this is largely due to the presence of organic materials in the charge transport layers and photoactive layer. Also, the lead (Pb) in the lead-based halide PSC is not environmentally friendly, and also it is water-soluble, which can lead to serious environmental issues if the encapsulation process is compromised. In an attempt to solve this issue, many researchers have attempted to replace the Pb content in the PSCs with other elements, such as tin and bismuth (Asif et al., 2025; Obi et al., 2021).

Beyond the photoactive layers, the charge transport layers (CTL) have been reported to influence the PCE and stability of PSCs. This is due to the fact that the hole transport layers (HTL) and the electron transport layers (ETL) and their interfaces are of great importance in controlling the collection and extraction of charges to the contacts (Akpaneno et al., 2024; Koech et al., 2021; Sanni et al., 2020). The CTLs also have impacts on the stability of PSCs. The inorganic CTLs have been reported to offer more stability than their organic counterpart, which is hydrophilic, which leads to interfacial degradation due to moisture at the interface of the CTLs and the photoactive layer. Many theoretical studies have been carried out, particularly in the Pb-based PSCs, to show that the HTL and ETL influence the PCE of PSCs (Adeniji et al., 2021; Akpaneno et al., 2024).

Several researchers have investigated lead-free perovskite solar cells (PSCs), including bismuth-based, tin-based, and germanium-based perovskites, as environmentally friendly alternatives to lead-containing absorbers (Asif et al., 2025; Atem & Makableh, 2025; Mortadi et al., 2024; Obi et al., 2021). Among these materials, germanium-based perovskites such as $CH_3NH_3GeI_3$ have attracted significant interest because of their suitable bandgap, strong optical absorption, and reduced toxicity. However, their practical implementation remains challenging due to the instability of Ge^{2+} ions, which readily oxidize to Ge^{4+} when exposed to ambient conditions. This oxidation process can introduce defect states, increase non-radiative recombination losses, degrade charge transport properties, and ultimately reduce device efficiency and long-term stability. Consequently, improving device architecture and understanding the factors that influence the performance of Ge-based PSCs are essential for advancing their viability.

Although germanium-based perovskites offer promising environmental advantages, critical knowledge gaps remain regarding their optimal device architecture with inorganic transport layers. Specifically, the effects of ZnO electron transport layer thickness and bandgap on photovoltaic performance remain underexplored for $CH_3NH_3GeI_3$ absorbers. Furthermore, the thermal behaviour and temperature-dependent performance degradation of such devices under realistic operating conditions have not been systematically investigated through numerical modelling, to the best of our knowledge. Therefore, this study addresses these gaps by performing a comprehensive SCAPS-1D optimization of ZnO ETL parameters, absorber properties, and temperature effects (290–360 K) in an FTO/ZnO/$CH_3NH_3GeI_3$/CuI/Au solar-cell structure.

In this paper, $CH_3NH_3GeI_3$-based PSCs with ZnO ETLs are thoroughly numerically studied using SCAPS-1D. To discover the most optimal design, the ZnO ETL thickness (10–400 nm) and band gap (2.0–4.0 eV) as well as the perovskite absorber thickness (300–800 nm) and band gap (1.2–1.6 eV) are varied. Subsequently, the optimized cell was simulated to investigate the thermal stability of the device by varying the temperature from 290 K to 360 K. The design of Ge-based PSCs and their viability under realistic operating conditions are guided by this thorough optimization.

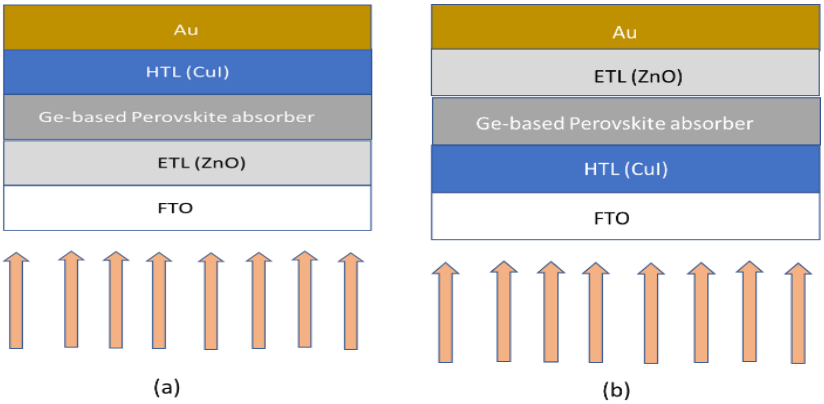

Figure 1: (a) the Regular n-i-p Architecture; (b) Inverted Planar p-i-n Architecture

MATERIALS AND METHODS

Solar Cell Structure for the Study

The solar cell architecture adopted for this study is the regular n-i-p structure of FTO glass/znO/Ge-based perovskite absorber/CuI/Au, as shown in figure 2. In this architecture light enters the solar cell from the ETL. Both ETL and HTL are inorganic materials. The Ge-based perovskite absorber is sandwiched between the two inorganic charge transport layers (CTLs), namely zinc oxide (ZnO) and copper iodide (CuI). Other layers are the transparent conducting oxide (TCO); in this study, we use FTO as the TCO and back contact.

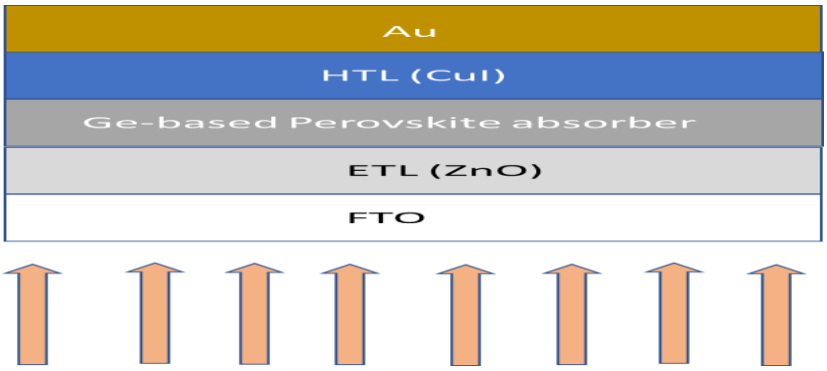

Figure 2: Proposed Solar Cell Structure

Numerical Simulation

Numerical analysis describes the fundamental phenomena seen in photovoltaic systems, allowing for intuitive study of each of the parameters in solar cells and thereby determining the ideal operating conditions. SCAPS-1D, a simulation software developed by the University of Ghent in Belgium, was used for this investigation. SCAPs-1D simulations are essentially based on two fundamental equations: the Poisson equation and the continuity equations for electrons and holes (Atem & Makableh, 2025).

$$\frac{d^2\phi(x)}{dx^2} = \frac{q}{\varepsilon_o \varepsilon_r}\left(p(x) - n(x) + N_D - N_A + \rho_p - \rho_n\right) \quad (1)$$

$$\frac{dn_n}{\mathrm{dt}} = \mathrm{G} - R \quad (2)$$

$$\frac{dn_p}{\mathrm{dt}} = \mathrm{G} - \mathrm{R} \quad (3)$$

$$J = J_n + J_p \quad (4)$$

$$J_n = qD_n\frac{dn}{dx} + q\mu_n n\frac{d\phi}{dx} \quad (5)$$

$$J_p = qD_p\frac{dp}{dx} + q\mu_p p\frac{d\varphi}{dx} \quad (6)$$

$$\alpha(\lambda) = (A + \frac{B}{h\upsilon})\sqrt{(h\upsilon - E_g)} \quad (7)$$

Where the symbols ε_0 and ε_r are the vacuum dielectric constant and the relative dielectric constant, respectively. The n and p represent the concentration of free carriers for electrons and holes, respectively. N_D is the concentration of donor impurity, and N_A represents the acceptor impurity. The charge densities of electrons and holes are denoted by ρ_n and ρ_p, respectively, whereas the current densities are denoted by Jn and Jp. The parameters R represent electron and hole recombination rates, whereas G denotes electron or hole creation rates. $\boldsymbol{\phi}$ represents the electric field, and q is the electrical charge, with a typical value of around 1.602 10^{-19} C. Electron and hole mobilities are given as μn and μp, respectively. Dp and Dn are the diffusion coefficients for free holes and electrons, respectively. The variable υ indicates optical frequency, while A and B are arbitrary constants. Eg denotes the bandgap, h Planck's constant, and α(λ) the absorption coefficient.

The Solar Cell Capacitance Simulator (SCAPS-1D) software was employed to perform all numerical simulations under standard AM1.5G illumination at 1000 W/m^2 and 300 K.

Table 1: Parameters of Different Layers (Asif et al., 2025; Atem & Makableh, 2025; Mortadi et al., 2024; Obi et al., 2021)

Parameters	FTO	ZnO (ETM)	$CH_3NH_3GeI_3$	CuI (HTM)
Thickness (nm)	300	10-400	300–800	300
Band gap (eV)	3.5	3.3	1.2–1.8	3.1
Electron affinity (eV)	4	3.9	4	2.1
Dielectric permittivity (relative), εr	9	9	18.00	6.5
Conduction band effective density of state (1/cm3)	2.200E+18	1.000E+19	1.000E+19	2.500E+20
Valence band effective density of state (1/cm3)	1.800E+19	1.000E+19	1.000E+19	2.500E+20
Electron thermal velocity (cm/s)	1.000E+7	1.000E+7	1.000E+7	1.000E+7
Hole thermal velocity (cm/s)	1.000E+7	1.000E+7	1.000E+7	1.000E+7
Electron mobility (cm2/V.s)	20	50	20.00	44
Hole mobility (cm2/V.s)	10	5	20.00	44
Donor concentration ND (1/cm3)	1.000E+18	1.000E+18	2.000E+16	0
Acceptor concentration NA (1/cm3)	0	0	2.000E+16	3.000E+18
Defect density Nt (1/cm3)	1.000E+15	1.000E+15	1.000E+15	1.000E+15

RESULTS AND DISCUSSION

Effect of Active Layer Thickness

To examine the effect of the photoactive layer thickness, simulations were performed on the structure shown in Fig. 2. The layer thickness was varied from 300 nm to 800 nm. Fig. 3 and table 2 presents the photovoltaic parameters, including the open circuit voltage (Voc), short circuit current density (Jsc), fill factor (FF), and power conversion efficiency (PCE), as functions of absorber layer thickness.

Fig. 3(a) shows the variation of Voc with absorber layer thickness. The result indicates that Voc decreases as absorber thickness increases, due to an increase in the dark saturation current. This behaviour is attributed to enhanced bulk recombination, as thicker films result in longer transport paths and reduced charge extraction efficiency. Similar trends have been widely reported in the literature (Liu et al., 2013). These effects are more pronounced in Ge-based perovskite solar cells due to their higher defect density and the instability of Ge^{2+} or Ge^{4+}.

Fig. 3(b) illustrates the performance of Jsc with absorber layer thickness. It is observed that Jsc increases with increasing thickness, owing to improved optical absorption and photogeneration. This trend is consistent with previous studies (Green et al., 2014).

Fig. 3(c) presents the variation of FF with absorber layer thickness. The findings indicate a monotonic decline with increasing thickness. This decrease can be explained by both greater recombination losses that lower charge extraction efficiency and increased series resistance linked to thicker films. This behaviour reflects mobility constraints within the absorber layer and indicates non-ideal charge transport characteristics.

Fig. 3(d) shows the variation of PCE with absorber layer thickness. The PCE initially increases, reaches a maximum, and then decreases. This behaviour reflects a trade-off between carrier generation and recombination. In the thin absorber region, low absorption results in reduced Jsc and PCE. At intermediate thickness, an optimal balance between absorption and recombination is achieved, leading to maximum PCE. However, at higher thicknesses, recombination losses dominate, resulting in serious reductions in Voc and FF and consequently lowering the PCE. The optimal absorber thickness is found in the range of around 500 nm–600 nm. The existence of an optimal absorber thickness arises from the trade-off between improved light absorption and increased recombination losses. Thicker films improve photogeneration, but they also lower Voc and FF because of bulk recombination and resistance losses.

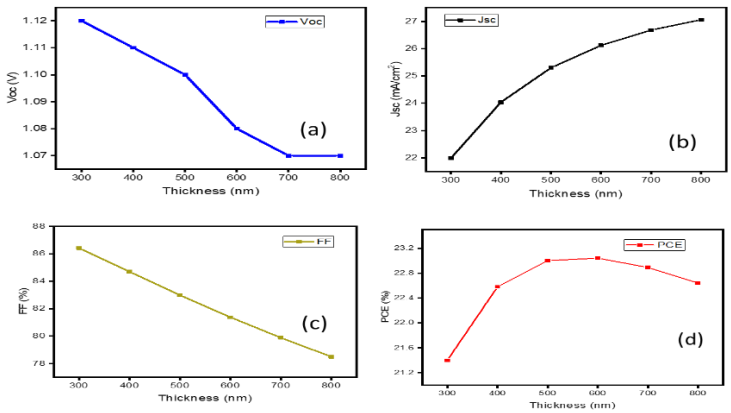

Figure 3: Effect of Ge-based Absorber Layer Thickness on the Photovoltaic Performance

Table 2: Impact of Photoactive Layer Thickness on the Photovoltaic Performance at 1.5 eV

S/N	Thickness (nm)	Voc (V)	Jsc (mA/cm^2)	FF (%)	PCE (%)
1	300	1.12	21.99	86.42	21.40
2	400	1.11	24.04	84.70	22.58
3	500	1.10	25.30	82.99	23.00
4	600	1.08	26.12	81.38	23.04
5	700	1.07	26.68	79.89	22.89
6	800	1.07	27.06	78.50	22.64

Effect of Absorber Layer Band Gap

To investigate the effect of the absorber layer bandgap on the photovoltaic parameters, simulations were performed on the structure shown in Fig. 2. The absorber bandgap was varied from 1.2 eV to 1.6 eV. Fig. 4 presents the variation of open circuit voltage (Voc), short-circuit current density (Jsc), fill factor (FF), and power conversion efficiency (PCE) as a function of the absorber bandgap.

Fig. 4(a) shows the variation of Voc with the absorber bandgap. It is observed that Voc increases monotonically with increasing bandgap. This behaviour indicates intrinsic carrier concentration and improved band alignment, leading to lower recombination losses and enhanced quasi-Fermi level splitting. This trend is consistent with established photovoltaic theory (Green et al., 2014).

Fig. 4(b) presents the variation of Jsc with absorber bandgap. The results indicate that Jsc decreases as the bandgap increases. This is attributed to the narrowing of the absorption spectrum at higher bandgaps, which limits photon absorption, particularly in the red and infrared regions, as explained by the Shockley-Queisser limit (Stranks et al., 2013).

Fig. 4 (c) shows the variation of FF with absorber bandgap. It is observed that FF initially increases and then decreases at higher bandgaps. At a lower bandgap, reduced recombination improves diode quality, leading to increased FF. However, at higher bandgaps, reduced carrier density and increased resistive losses result in a decline in FF. The non-monotonic results from the relationship of recombination and resistive losses, with improved diode properties at intermediate bandgaps and increasing transport constraints at higher bandgaps. Fig. 4(d) shows how PCE varies with absorber bandgap. The PCE initially rises, reaches a peak, and then drops sharply. At low bandgaps, the Jsc is large, but the Voc is low, reducing total efficiency. At an ideal bandgap, the balance of Jsc, Voc, and FF yields maximum PCE. At high bandgap, there is a considerable drop in Jsc, alongside the deterioration of FF, which leads to a sharp decline in PCE. The optimal bandgap is found to be in the range of 1.4 eV-1.5 eV, which is in agreement with the Shockley-Queisser limit of 1.34 eV.

Furthermore, Ge-based perovskite materials have a more pronounced PCE drop at higher bandgaps due to their higher defect density, shorter carrier lifetime, and increased recombination loss sensitivity.

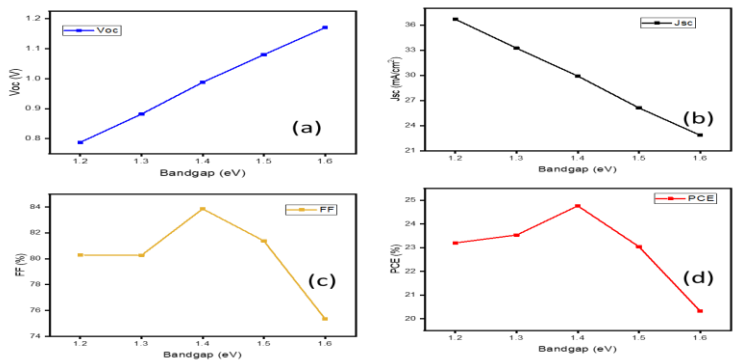

Figure 4: Effect of Ge-based absorber layer Band Gap on the Photovoltaic Performance

Table 3: Absorber Layer Band Gap Effect on the PSCs' Performance at 600 Nm Thickness

S/N	Band gap (eV)	Voc (V)	Jsc (mA/cm^2)	FF (%)	PCE (%)
1	1.2	0.788	36.69	80.29	23.20
2	1.3	0.882	33.24	80.27	23.53
3	1.4	0.988	29.92	83.86	24.76
4	1.5	1.08	26.12	81.38	23.04
5	1.6	1.17	22.86	75.35	20.32

Effect of ZnO Layer Thickness

In this section, the variation of photovoltaic parameters as functions of ZnO ETL thickness will be discussed. Fig. 5 and Table 4 show the results of the variation of Voc, Jsc, FF, and PCE with ZnO thickness.

The Voc and the FF remain constant for the entire ZnO ETL thickness range of 10 nm to 400 nm, maintaining values of approximately 0.987 V and 83.85% for Voc and FF, respectively, as shown in Fig. 5(a) and Fig. 5(c). The reason for this behaviour is attributed to the electrical conductivity of the ZnO due to its low resistivity of 1.25 x 10^{-4} Ωcm and idealized situation considered in this study without interfacial defect. As a result, even at a thickness of 400 nm, the contribution to series resistance remains very low, and the FF is not seriously affected. The second reason is because of the absence of interface recombination at the ZnO/perovskite interface, keeping the recombination velocity at zero. Consequently, Voc is governed by only the bulk recombination within the perovskite absorber, and it is independent of the ETL thickness.

Furthermore, the steady Voc across ZnO thickness indicates good band alignment between ZnO and the perovskite absorber. The depletion region spread mainly into the perovskite layer, making the ZnO thickness independent of the built-in potential.

Fig. 5(b) and (d) depict the changes of Jsc and PCE with ZnO thickness, respectively. The Jsc decreased by less than 1%, from 30.13 mA/cm^2 at 10 nm to 29.86 mA/cm^2 at 400 nm. The PCE shows a similar pattern, falling slightly from 24.93% to 24.17%. This decline is primarily due to parasitic absorption in the ZnO layer.

As the ZnO thickness increases, a smaller fraction of these photons get to the perovskite absorber, leading to a reduction in photogeneration.

This simulation shows that for ZnO-based perovskite solar cells under ideal conditions, the ZnO thickness can be varied for a wide range of thicknesses (10-400 nm) without seriously affecting the Voc and the FF, while it affects the Jsc marginally.

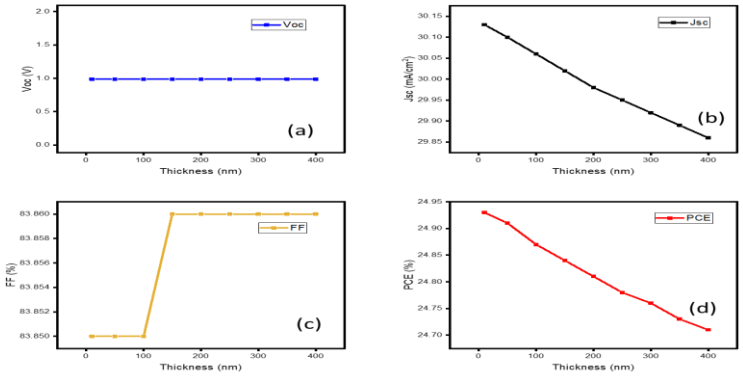

Figure 5: Effect of ZnO Thickness on the Photovoltaic Performance of Ge-Based Perovskite Solar Cells

Table 4: Effect of ZnO Layer Thickness on Photovoltaic Properties

S/N	Thickness (nm)	Voc (V)	Jsc (mA/cm^2)	FF (%)	PCE (%)
1	10	0.987	30.13	83.85	24.93
4	50	0.987	30.10	83.85	24.91
5	100	0.987	30.06	83.85	24.87
6	150	0.987	30.02	83.86	24.84
7	200	0.987	29.98	83.86	24.81
8	250	0.987	29.95	83.86	24.78
9	300	0.987	29.92	83.86	24.76
10	350	0.987	29.89	83.86	24.73
11	400	0.987	29.86	83.86	24.71

Effect of ZnO Band Gap

Fig. 6 presents the results of how varying the ZnO ETL bandgap affects Voc, Jsc, FF, and PCE.

Fig. 6(a) shows the variation of Voc with the ZnO layer bandgap. From the result, it is observed that the Voc remains constant across the entire ZnO bandgap range. This indicates that ETL has a negligible effect on the built-in potential, suggesting that there is a stable band alignment between ZnO and the perovskite absorber. Also, it suggests that no additional recombination is introduced at higher/lower ZnO bandgaps. This implies that Voc is governed only by bulk recombination and not ZnO energetics.

Fig. 6(b) shows the variation of Jsc with the ZnO bandgap. The result shows that Jsc increases slightly with an increase in the ZnO bandgap. This is a result of a reduction in parasitic absorption. Increasing the ZnO bandgap shifts the absorption edge to a shorter wavelength and makes ZnO more transparent. Which implies that more photons get to the absorber layer; increasing the photogeneration implies improved Jsc.

Fig. 6 (c) shows the result of the variation of FF with the ZnO bandgap. It is observed that the FF remains constant for the entire range of the ZnO bandgap. This indicates that there is no significant change in the series resistance, charge transport efficiency, and recombination pathway. Which suggests that electron extraction is efficient across the entire ZnO range of bandgaps, which implies no barrier formation at the interface.

Fig. 6(d) shows the variation of PCE with ZnO bandgap. It is observed that the PCE increases sharply initially, then saturates. PCE increases initially; this suggests that increasing the ZnO bandgap improves the conduction band alignment, reduces interface recombination, and enhances electron selectivity. At the saturation region, beyond a certain bandgap, the improvement in the Voc, Jsc, and FF, and hence the PCE, plateaus.

Table 5: Effect of ZnO Band Gap

S/N	Band gap (eV)	Voc (V)	Jsc (mA/cm^2)	FF (%)	PCE (%)
1	2.0	0.987	30.09	83.85	24.9
2	2.5	0.987	30.11	83.85	24.92
3	3.0	0.987	30.12	83.85	24.93
4	3.5	0.987	30.12	83.85	24.93
5	4.0	0.987	30.12	83.85	24.93

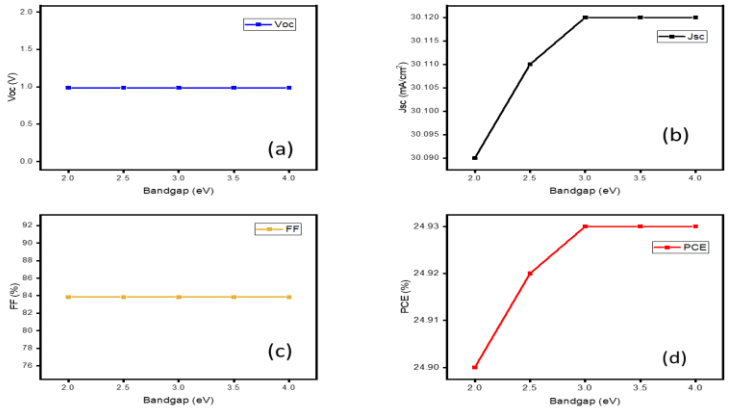

Figure 6: Effect of ZnO ETL Band Gap on the Performance of Ge-based PSCs

Effect of Temperature on the Photovoltaic Performance

Fig. 7 illustrates how increasing temperature affects Voc, Jsc, FF, and PCE. The variation of Voc with temperature is shown in Fig. 7(a). It is observed that Voc decreases linearly with increasing temperature; this obeys the thermal effect relation. As temperature increases, the saturation current increases exponentially, the bandgap slightly decreases, and carrier recombination increases. This leads to a reduction in the quasi-Fermi level and a significant drop in Voc (Shockley & Queisser, 1961). It indicates strong recombination sensitivity in Ge-based PSCs.

Fig. 7(b) presents the variation of Jsc with temperature. It is observed that the Jsc remains approximately constant. Although theory suggests that temperature can increase absorption and carrier generation. However, in our simulation it does not obey the theory; this is because (i) absorption is already near saturation, (ii) optical properties of SCAPS are weakly temperature dependent, and (iii) carrier collection is not limiting since transport layers are optimized and electric field is sufficient. This behaviour is physically consistent for ideal, well-optimized devices (Jenny Nelson, 2003; Wolfgang Tress, 2017).

Fig. 7(c) shows the variation of FF with temperature. The curve shows that FF decreases steadily with increasing temperature. As the temperature rises, recombination losses rise, series resistance rises, and the diode identity decreases, resulting in lower charge extraction efficiency. This suggests transport deterioration and increases non-ideal behaviour. (Wolf et al., 2014).

From Fig. 7(d), PCE decreases with temperature; this is dominated by Voc and FF since Jsc is constant.

As a result, the PCE drops significantly with increasing temperature. The drop in PCE arises mainly from the Voc and the FF since the Jsc remains fairly constant. This trend agrees with both theoretical predictions and practical results in PSCs, where temperature effects mainly affect the recombination dynamics instead of the photogeneration (Shockley & Queisser, 1961; Wolfgang Tress, 2017).

The results show that thermal instability of Ge-based PSCs is mainly caused by recombination and transport losses, rather than optical restrictions. This could be due to the fact that Ge-based materials exhibit higher defect concentrations and shorter carrier lifetimes compared to Pb-based perovskite materials (Hao et al., 2014; Krishnamoorthy et al., 2015).

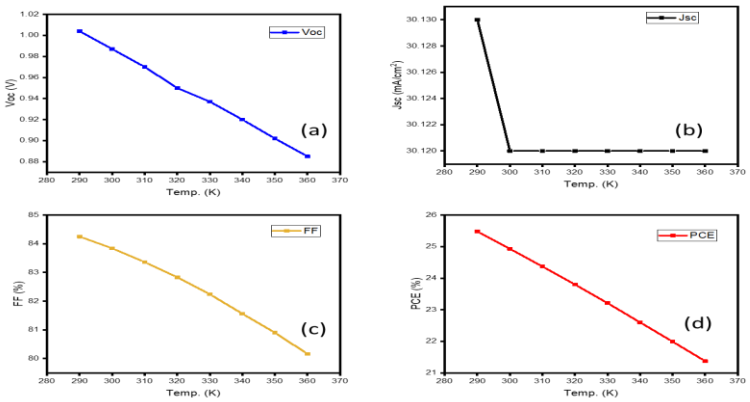

Figure 7: Effect of Temperature on the Performance of the Optimized of Ge-based Perovskite Solar Cells

Table 6: Effect of Temperature on Photovoltaic Performance of Ge-Based PSCs

S/N	Temperature (K)	Voc (V)	Jsc (mA/cm^2)	FF (%)	PCE (%)
1	290	1.004	30.13	84.25	25.48
2	300	0.987	30.12	83.84	24.93
3	310	0.970	30.12	83.36	24.37
4	320	0.950	30.12	82.83	23.80
5	330	0.937	30.12	82.24	23.21
6	340	0.920	30.12	81.56	22.60
7	350	0.902	30.12	80.90	21.99
8	360	0.885	30.12	80.16	21.37

CONCLUSION

In this work, a numerical investigation of a lead-free germanium-based perovskite solar cell with the structure FTO/ZnO/$CH_3NH_3GeI_3$/CuI/Au was carried out using SCAPS-1D simulation software. The effects of absorber layer thickness, absorber bandgap, ZnO electron transport layer (ETL) thickness, ZnO bandgap, and operating temperature on the photovoltaic performance were systematically analysed.

The results revealed that the absorber layer thickness strongly influences the device performance due to the trade-off between optical absorption and recombination losses. An optimum absorber thickness in the range of 500–600 nm produced the best performance with a PCE of about 23–24%. Similarly, the absorber bandgap significantly affected the photovoltaic parameters, with the optimal bandgap found between 1.4 and 1.5 eV, yielding a maximum PCE of approximately 24.9%. Lower bandgaps enhanced Jsc but reduced Voc, whereas higher bandgaps improved Voc at the expense of carrier generation.

The study further demonstrated that the ZnO ETL thickness has only a marginal influence on Voc and FF due to the excellent conductivity and favourable band alignment of ZnO. However, thicker ZnO layers slightly reduced Jsc and PCE because of parasitic absorption. Increasing the ZnO bandgap improved transparency and slightly enhanced Jsc and PCE, while Voc and FF remained nearly constant across the investigated range.

Temperature analysis showed that increasing operating temperature from 290 K to 360 K leads to a considerable reduction in Voc, FF, and PCE, whereas Jsc remains nearly unchanged. This behaviour confirms that thermal degradation in Ge-based PSCs is mainly governed by recombination and transport losses rather than optical limitations. The optimized device achieved a maximum PCE of about 25.48% at 290 K, which decreased progressively with increasing temperature.

Overall, the findings demonstrate that proper optimization of inorganic transport layers and absorber properties can significantly improve the efficiency and thermal stability of lead-free germanium-based perovskite solar cells. The study provides valuable insights into the design of environmentally friendly and thermally robust PSCs and highlights the potential of ZnO-based inorganic transport layers for future high-performance lead-free perovskite photovoltaic applications.

It should be noted that the present study is based on SCAPS-1D simulations and assumes idealized interfaces and defect distributions. Consequently, the effects of interface imperfections, fabrication-induced defects, and Ge^{2+} oxidation-related degradation are not fully captured in the model. Future work should therefore focus on the experimental realization of the optimized device architecture, interface engineering strategies to suppress recombination losses, and detailed stability investigations under thermal, moisture, and illumination stress conditions to assess the practical viability of $CH_3NH_3GeI_3$-based perovskite solar cells.

REFERENCES

Adeniji, S., Oyewole, O., Koech, R., Oyewole, D., Cromwell, J., Ahmed, R., Oyelade, O., Sanni, D., Orisekeh, K., Bello, A., & Soboyejo, W. (2021). Failure Mechanisms of Stretchable Perovskite Light-Emitting Devices under Monotonic and Cyclic Deformations. *Macromolecular Materials and Engineering*, *306*(11). https://doi.org/10.1002/mame.202100435

Akpaneno, F. A., Sanni, D. M., & Salim, M. A. (2024). Theoretical Study of Inorganic Charge Transport Layer of Perovskite Solar Cells Using Scaps Software. *Physical Science International Journal*, *28*(4), 57–63. https://doi.org/10.9734/psij/2024/v28i4837

Asif, P., Chetia, A., Saikia, D., & Sahu, S. (2025). A comprehensive theoretical investigation of lead-free mixed

antimony-bismuth halide double perovskite ($Cs_2AgBi_{0.75}Sb_{0.25}Br_6$) solar cell using SCAPS-1D. *Discover Electronics*, *2*(1). https://doi.org/10.1007/s44291-025-00085-8

Atem, M. Al, & Makableh, Y. (2025). Towards Sustainable Perovskite Solar Cells : Lead-Free High Efficiency Designs with Tin and Germanium. *Eng MDPI*, *6*(38).

Green, M. A., Ho-Baillie, A., & Snaith, H. J. (2014). The emergence of perovskite solar cells. *Nature Photonics*, *8*(7), 506–514. https://doi.org/10.1038/nphoton.2014.134

Hao, F., Stoumpos, C., & D. Cao, R. Chang, M. K. (2014). Lead-Free Solid-State Organic-Inorganic Halide Perovskite Solar Cells. *Nature Photonics*, *8*, 489–494. https://doi.org/10.1038/nphoton.2014.82

Jenny Nelson. (2003). *The Physics of Solar Cells. Imperial College Press, London.* https://doi.org/10.1142/p276

Kim, H. S., Lee, C. R., Im, J. H., Lee, K. B., Moehl, T., Marchioro, A., Moon, S. J., Humphry-Baker, R., Yum, J. H., Moser, J. E., Grätzel, M., & Park, N. G. (2012). Lead iodide perovskite sensitized all-solid-state submicron thin film mesoscopic solar cell with efficiency exceeding 9%. *Scientific Reports*, *2*, 1–7. https://doi.org/10.1038/srep00591

Koech, R. K., Ichwani, R., Oyewole, D. O., Kigozi, M., Amune, D., Sanni, D. M., Adeniji, S. A., Oyewole, O. K., Bello, A., Ntsoenzok, E., & Soboyejo, W. O. (2021). Tin oxide modified titanium dioxide as electron transport layer in formamidinium-rich perovskite solar cells. *Energies*, *14*(23), 1–13. https://doi.org/10.3390/en14237870

Krishnamoorthy, T., Ding, H., Yan, C., Leong, W. L., Baikie, T., Zhang, Z., Sherburne, M., Li, S., Asta, M., & Nripan Mathews and Subodh G. Mhaisalkar. (2015). Lead-free germanium iodide perovskite materials for photovoltaic applications. *Journal of Materials Chemistry A*, *3*(47), 23829–23832. https://doi.org/org/10.1039/C5TA05741H

Lee, M. M., Teuscher, J., Miyasaka, T., Murakami, T. N., & Snaith, and H. J. (2012). Efficient Hybrid Solar Cells Based on Meso-Superstructured Organometal Halide Perovskites. *Science*, *338*(6107), . 643-647. https://doi.org/10.1126/science.122860

Liu, M., Johnston, M. B., & Snaith, H. J. (2013). Efficient planar heterojunction perovskite solar cells by vapour deposition. *Nature*, *501*(7467), 395–398. https://doi.org/10.1038/nature12509

Mortadi, A., El Hafidi, E., Nasrellah, H., Monkade, M., & El Moznine, R. (2024). Analysis and optimization of lead-free perovskite solar cells: investigating performance and electrical characteristics. *Materials for Renewable and Sustainable Energy*, *13*(2), 219–232. https://doi.org/10.1007/s40243-024-00260-z

National Renewable Energy Laboratory (NREL). (2025). *Best research-cell efficiency chart.*

Obi, U. C., Sanni, D. M., & Bello, A. (2021). Effect of Absorber Layer Thickness on the Performance of Bismuth-Based Perovskite Solar Cells. *Semiconductors*, *55*(12), 922–927. https://doi.org/10.1134/S1063782621040114

Sanni, D. M., Chen, Y., Yerramilli, A. S., Ntsoenzok, E., Asare, J., Adeniji, S. A., Oyelade, O. V., Fashina, A. A., & Alford, T. L. (2019). An approach to optimize pre-annealing aging and anneal conditions to improve photovoltaic performance of perovskite solar cells. *Materials for Renewable and Sustainable Energy*, *8*(1), 1–10. https://doi.org/10.1007/s40243-018-0139-3

Sanni, D. M., Joseph, E., Aminu, M., & Adamu. (2020). The importance of Film Thickness on the Photovoltaic Performance of Perovskite Solar Cells. *Fudma Journal of Sciences*, *4*(1), 600–606.

Sanni, D. M., Yerramilli, A. S., Ntsoenzok, E., Adeniji, S. A., Oyelade, O. V., Koech, R. K., Fashina, A. A., & Alford, T. L. (2021). Impact of precursor concentration on the properties of perovskite solar cells obtained from the dehydrated lead acetate precursors. *Journal of Vacuum Science & Technology A: Vacuum, Surfaces, and Films*, *39*(3). https://doi.org/10.1116/6.0000714

Shockley, W., & Queisser, H. J. (1961). Detailed Balance Limit of Efficiency of p-n Junction Solar Cells. *Journal of Applied Physics*, *33*(3), 510–519. https://doi.org/org/10.1063/1.1736034

Stranks, S. D., Eperon, G. E., Grancini, G., Menelaou, C., & Snaith, H. J. (2013). Electron-Hole Diffusion Lengths Exceeding Trihalide Perovskite Absorber. *Science*, *342*(October), 341–344. https://doi.org/10.1126/science.1243982

Wolf, S. De, Holovsky, J., Moon, S.-J., Löper, P., Niesen, B., Ledinsky, M., Haug, F.-J., Yum, J.-H., & Ballif, C. (2014). Organometallic Halide Perovskites: Sharp Optical Absorption Edge and Its Relation to Photovoltaic Performance. *The Journal of Physical Chemistry Letters*, *5*(6), 1035–1039. https://doi.org/org/10.1021/jz500279b

Wolfgang Tress. (2017). Perovskite Solar Cells on the Way to Their Radiative Efficiency Limit – Insights Into a Success Story of High Open-Circuit Voltage and Low Recombination. *Advanced Energy Materials*, *7*(14), 1602358. https://doi.org/org/10.1002/aenm.201602358Digital Object Identifier (DOI)

Xing, G., Mathews, N., Lim, S. S., Lam, Y. M., Mhaisalkar, S., & Sum, T. C. (2013). *Long-Range Balanced Electron- and Hole-Transport Lengths in Organic-Inorganic CH 3 NH 3 PbI 3*. *6960*(October), 498–500.